www.czasopisma.pan.pl PAN POLSKA AKADEMIA NAUK www.journals.pan.pl

Arch. Metall. Mater. **67** (2022), 3, 921-930

DOI: https://doi.org/10.24425/amm.2022.139684

EBENEZER GEORGE[1], ADAM KHAN M.[1]*, CHELLAGANESH DURAIPANDI[1], WINOWLIN JAPPES J.T.[1], JULFIKAR HAIDER[2]

ASSESSING MACHINABILITY AND SURFACE CHARACTERISTICS OF A SHAPE MEMORY ALLOY (SMA) PROCESSED THROUGH WIRE ELECTRO SPARK EROSION METHOD

In this paper, a study was carried out to investigate the surface roughness and material removal rate of low carbon NiTi shape memory alloy (SMA) machined by Wire Electro Spark Erosion (WESE) technique. Experiments are designed considering three parameters viz, spark ON time (S_{ON}), spark OFF time (S_{OFF}), and voltage (V) at three levels each. The surface roughness increased from 2.1686 µm to 2.6869 µm with an increase in both S_{ON} time, S_{OFF} time and a decrease in voltage. The material removal rate increased from 1.272 mm^3/min to 1.616 mm^3/min with an increase in S_{ON} time but a varying effect was observed the S_{OFF} time and voltage were varied. The analysis revealed that the intensity and duration of the spark had an unswerving relation with the concentration of the microcracks and micropores. More microcracks and micropores were seen in the combination of S_{ON} = 120 µs, voltage = 30 V. The concentration of the microcracks and micropores could be minimised by using an appropriate parameter setting. Therefore, considering the surface analysis and material removal, the low carbon NiTi alloy is recommended to machine with 110 µs – 55 µs – 30 v (S_{ON} – S_{OFF} – V respectively), to achieve better surface roughness with minimal surface damage.

Keywords: Wire Electro Spark Erosion; Machining; NiTi alloy; Surface roughness; Material removal rate (MRR)

1. Introduction

Functional materials (FMs) have an enhanced mechanical and thermal properties placed itself in contributing towards satisfying the societal needs. In the current scenario, tremendous growth in the robotics, aerospace, automotive, nuclear, and biomedical sectors have opened up a lot of opportunities for the scientists and researchers towards bringing new innovations in the field of materials and manufacturing [1]. The FMs as a state-of-the-art material have palpable characteristics such as electrochemical, wear, bio-compatibility, fatigue, super elasticity, elevated temperature applicability etc. [2,3]. The FM's attractive and multidimensional properties made them commercially available for viable applications. Some of the FMs viz, Udimet-L60, Nimonic C-263, Nimonic-75, Inconel 718, Ti-5Al-2.5Sn, TITAN 15 ASTM Grade 2, TITAN 21 ASTM Grade 6, $Ni_{50}Ti_{40}Cu_{10}$, $Ni_{50}Ti_{45}Co_5$, $Ni_{55.74}Ti_{44.26}$, $Ni_{49.3}Ti_{50.7}$, SE508 Nitinol of composition $Ni_{50.8}Ti_{49.2}$, $Ni_{55.95}Ti_{44.05}$, and $Ni_{40}Ti_{60}$ have been considered for studies by various researchers. The Ni-Ti based FMs demonstrated better tribological, fatigue, and super elastic properties [4-13].

Nickel-Titanium (Ni-Ti) shape memory alloy (SMA) is commercially available in various grades to suit the requirements of specific applications. The Ni-Ti alloy needs to be machined for changing its shape and size to fit applications such as automotive and biomedical where surface quality, dimensional accuracy and productivity of the machined part are the major concerns. The Ni-Ti alloy machined by conventional techniques resulted in longer machining time, poorer surface quality and inferior dimensional accuracy [14]. The unfavorable results of the conventional techniques forced the industries to adopt unconventional machining strategies. Electro Spark Erosion (ESE) technique familiarized as electric discharge machining has an ability to create better surface quality and dimensionally accurate components [15,16]. The ESE technique removes the material by means of thermal energy generated by the spark between the electrode and the workpiece at regular intervals. Wire Electro Spark Erosion (WESE), and Micro Electro Spark erosion (µESE) are variants of the electro spark erosion technique. Even though ESE technique has primary advantages towards machining FMs, there are still some challenges left such as deposition of molten material over the machined surface, formation of microcracks and micropores,

[1] SCHOOL OF AUTOMOTIVE AND MECHANICAL ENGINEERING AND CENTRE FOR SURFACE ENGINEERING, KALASALINGAM ACADEMY OF RESEARCH AND EDUCATION, TAMIL NADU, INDIA
[2] MANCHESTER METROPOLITAN UNIVERSITY, ADVANCED MATERIALS AND SURFACE ENGINEERING (AMSE) RESEARCH CENTRE, CHESTER STREET, M1 5GD, UK
* Corresponding author:

deposition of undesirable elements, etc. These challenges in the machining need to be addressed by appropriate investigation.

The WESE is commonly employed for machining Ni-Ti alloys specified for the bio medical applications. The machining performance and the quality of the machined surface produced by the WESE process depend on machine parameters viz, pulse on time, pulse off time, gap voltage, peak current, dielectric medium, wire feed rate, wire material, wire tension, spark frequency, flushing pressure, etc. [17-19]. The attributes commonly employed for measuring performance and the surface quality are Material Removal Rate (MRR) and Surface Roughness (SR) respectively [20]. The Ni-Ti alloy machined by WESE technique revealed that the pulse ON time, gap voltage, wire feed and pulse OFF time could significantly affect SR and MRR [21-24]. Some researchers also found that the deposition of molten material over the surface during the WESE process affected the electrochemical behaviour of the workpiece material. The WESE process also induced the formation of thermal cracks over the machined surface. The WESE process erodes the material by means of melting it and due to the application of high thermal energy, thermal stresses generated on the machined surface leads to surface cracks, pores and voids.

Machinability of nickel alloys and titanium alloys are available in literature to discuss about the merits and demerits for different types of machining process. Especially, these alloys are difficult to machine with edge cutting tool processes. In this paper, the novelty of the research is to focus on machining of low carbon nickel – titanium – based shape memory alloy. The low carbon NiTi alloy is a modified alloy, which is different from the commercially available NiTi shape memory alloys. The presence of carbon in NiTi alloy supports to enrich the mechanical strength and resistance towards wear, erosion and corrosion. Hence, an attempt is made to study the machinability of low carbon NiTi alloy using wire electro spark erosion method (WESE aka WEDM). The findings from the machining studies may support researchers and lead to recommend the use wire electro spark erosion machined low carbon NiTi alloy for biomedical application. Based on the challenges faced during the machining of low carbon NiTi alloy; the surface defects, micropores, microcracks, cast layer deposition are explored the reasons for the defect generation and made suggestions for minimizing the surface defects without compromising the productivity. As a summary, the literatures are available to report the machinability of non – ferrous metals with wire electrical discharge machining is available [25,26]. It has been confirmed that the alloying elements in the base material in relation the machining process condition decides the surface quality and material removal during machining [21,27,28]. Hence an attempt made to study the machinability of nickel titanium carbon alloy using wire electro spark process.

The aim of the research is to investigate the machinability of low carbon nickel titanium alloy using wire electro spark erosion process. From the investigation, the rate of material removal and surface finish are studied to evaluate the machining performance. Materials characterization technique is used report the surface quality of the machined material.

2. Experimental procedure

2.1. Shape memory alloy material

The low carbon NiTi alloy considered for experimentation was a circular rod of diameter 15 mm procured from Ultimate Enterprise, Tamilnadu, India. The procured low carbon NiTi alloy was cleaned with acetone before machining to eradicate any undesirable elements over the surface. The element weight percentage of the alloy has been confirmed through the optical emission spectroscopy and the details are given in the TABLE 1.

Major alloying element has been confirmed through the spectroscopic analysis and the sub – elements are very meager in the level of traces. The vertical microscope (Make: Vertimet, Chennai METCO) is used to study and record the microstructure of the alloy. Fig. 1a shows the microstructure of low carbon NiTi

TABLE 1

Elemental distribution in NiTi alloy

Element	Ni	Ti	C	Co	Fe	Al	Cr	Cu, Mo, Si
wt. %	51.80	46.356	0.052	0.352	0.188	0.134	0.469	Traces

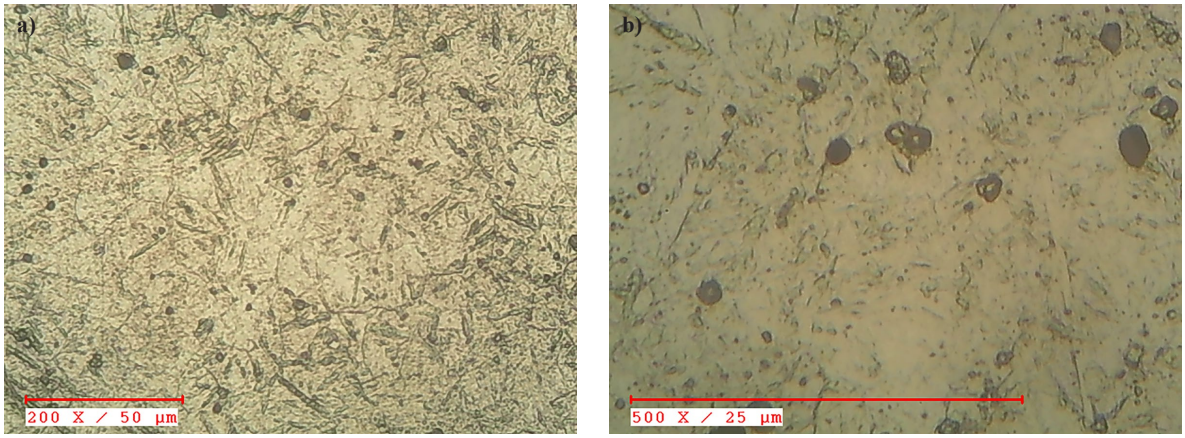

Fig. 1. Optical images of low carbon NiTi alloy used for WESE machining studies at (a) lower magnification and (b) higher magnification

alloy. In the optical image, the carbon elements are found in the form of spheroids over the austenitic phase as in the Fig. 1b. The distribution of carbon found uniform throughout the alloy as confirmed through the microstructural report. The properties of the materials are as follows: density – 6.48 g/cm^3, yield strength – 695 MPa and ultimate tensile strength – 891 MPa with a micro hardness 341 Hv.

2.2. Machining procedure

The machining process was carried out in the Electronica CNC wire cut discharge machine and experimental set-up of the WESE process is presented in Fig. 2. The set-up utilized 0.25 mm electrode wire as a tool for the machining process. The half hard brass wire is procured from a standard supplier (Mending Metals, India) with an alloying composition of Cu – 60% and Zn – 40% respectively. In view with literature, three input process parameters viz, Spark ON time (S_{ON}), Spark off time (S_{OFF}), and voltage (V) were chosen considering their influence towards the surface property and productivity. The levels of each parameters were decided by conducting the preliminary test towards the responses chosen. After the preliminary test, the chosen levels for each parameter are provided in TABLE 2. However, the other process conditions such as Potential input (230 V), Peak current (12 A), dielectric medium (Deionized water), wire feed rate (3 m/min), wire material (half hard copper wire), wire tension (7 kg /mm), cutting speed (1 mm/min) and the duty factor (90%) were maintained constant throughout the experimentations.

Machining has been done by sectioning low carbon NiTi alloy to a dimeter of 15 mm and a width of 5 mm as per the experimental design order. The sectioned low carbon NiTi alloy specimen by the WESE process is presented in the Fig. 3. During the WESE process the machining time for all the experiments were recorded. The machining time was further used to calculate the MRR for each specimen using the mathematical equation (Eq. 1).

$$MRR = \frac{CAS \times W}{MT} \tag{1}$$

Where, MRR is Material Removal Rate (mm^3/min), CSA is cross sectional area of the specimen (mm^2), W is width of the cut (mm) and MT is machining time (min).

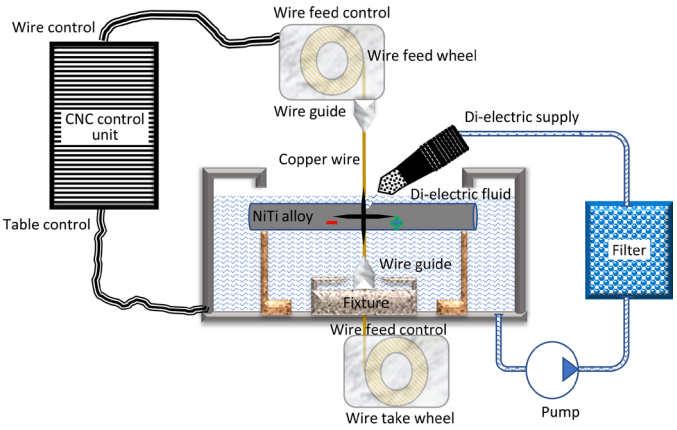

Fig. 2. Schematic arrangement of machining setup of WESE process

TABLE 2

Experimental attributes for WESE process

Serial No	Parameters	Notation	Units	Range
1	Spark ON time	S_{ON}	µs	110, 115, 120
2	Spark OFF time	S_{OFF}	µs	50, 55, 60
3	Voltage	Volt	v	10, 20, 30

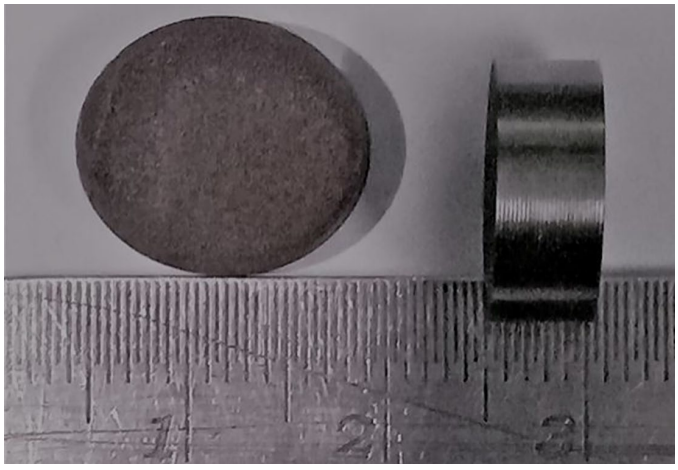

Fig. 3. Photographic image of a sectioned Ni-Ti specimen

2.3. Evaluation techniques of machining performance

After machining, the SR of the machined specimen was measured perpendicular to the direction of the wire feed by using Mitutoyo Surftest SJ410 roughness tester (with an accuracy of 0.01 µm) with a cut-off length of 8 mm. The SR values were measured as root mean square values (Ra) i.e. average deviation from the nominal surface. For each machined specimen, measurement was repeated three times to reduce the effect of uncontrollable parameters and the average of three measured values were taken as SR of the specimen.

The surface morphology of the machined specimen was studied under ZEISS EVO 18 scanning electron microscope. The elemental analysis of the machined surface and their mapping was carried out by using a Bruker's energy dispersive spectroscopy attached with the ZEISS EVO 18 SEM.

3. Results and Discussions

3.1. Surface roughness

The SR value of the machined specimens varied within a range between 2.168 µm-2.686 µm. The minimum SR value (2.168 µm) was observed at a machining condition of

S_{ON} = 110 µs, S_{OFF} = 50 µs, and voltage = 30 V whereas, the maximum SR value (2.686 µm) was found at a machining condition of S_{ON} = 120 µs, S_{OFF} = 60 µs, and voltage = 10 V. To better understand the relationships among $S_{ON,}$ $S_{OFF,}$ and voltage in relation to SR, three graphs were plotted. The graph shown in Fig. 4(a) plotted between the S_{ON} time and SR by keeping the other parameters constant. Similarly, Fig. 4(b) represents the graph plotted between the S_{OFF} time and SR by keeping the other two parameters constant. Finally, Fig. 4(c) presents the plot between V and SR by keeping the other two parameters constant. From the graph, it was clear that SR increased with an increase in S_{ON} and $S_{OFF,}$ but SR decreased with an increase in V. The SR increased with an increase in the spark ON time (S_{ON}), which increased the discharge energy due to the spark lasting for a longer period. This enabled the WESE process to erode more surface material which created more globules over the machined surface resulting in an increased surface irregularity. Similarly, SR decreased with an increase in voltage (V). Literature reports that the surface finish depends upon the pulse duration and power consumed for electro spark production [27]. This could be due to the fact that as the voltage increased, the intensity of the spark increased leading to complete melting of material that washed away by the flow of dielectric. Therefore, less surface irregularities were generated. The variation of the SR with respect to S_{OFF} time was less compared with S_{ON} time and voltage. In the future research scope, it has been planned to perform the investigation with varying wire feed rate to study the intensity spark generated. The surface lapping due to wire spark may have high influence to produce better surface finish while machining the hard material [28].

3.2. Material Removal Rate (MRR)

Likewise, the MRR value of the machined specimens varied within a range of 1.272 mm^3/min-1.616 mm^3/min. The minimum MRR value was obtained at the machining condition of S_{ON} = 110 µs, S_{OFF} = 50 µs, and voltage = 10 V. Similarly, the maximum MRR value was achieved at the machining condition of S_{ON} = 120 µs, S_{OFF} = 55 µs, and voltage = 30 V. To better understand the relationships among S_{ON}, S_{OFF}, and voltage in relation to MRR, three graphs were plotted. The graph shown in Fig. 5(a) plotted between the S_{ON} time and MRR by keeping the other parameters as constant. Similarly, Fig. 5(b) represented the graph plotted between the S_{OFF} time and MRR by keeping the other two parameters constant. Finally, Fig. 5(c) presented the plot between voltage and MRR by keeping the other two parameters constant. From the graph it was noticed that MRR increased with an increase in S_{ON} time but the MRR in relation to S_{OFF} time and voltage did not show any clear trend. The MRR increased with an increase in the spark ON time (S_{ON}), which increased the discharge energy as the spark lasted longer. This enabled the WESE process to erode additional surface material. On the other hand, the maximum MRR obtained at the maximum voltage (V) could be due to the fact that as the higher spark potential increased additional melting.

3.3. Machined surface characteristics

The machined surface was characterized using the SEM and presented in Fig. 6. From the images the formation of the

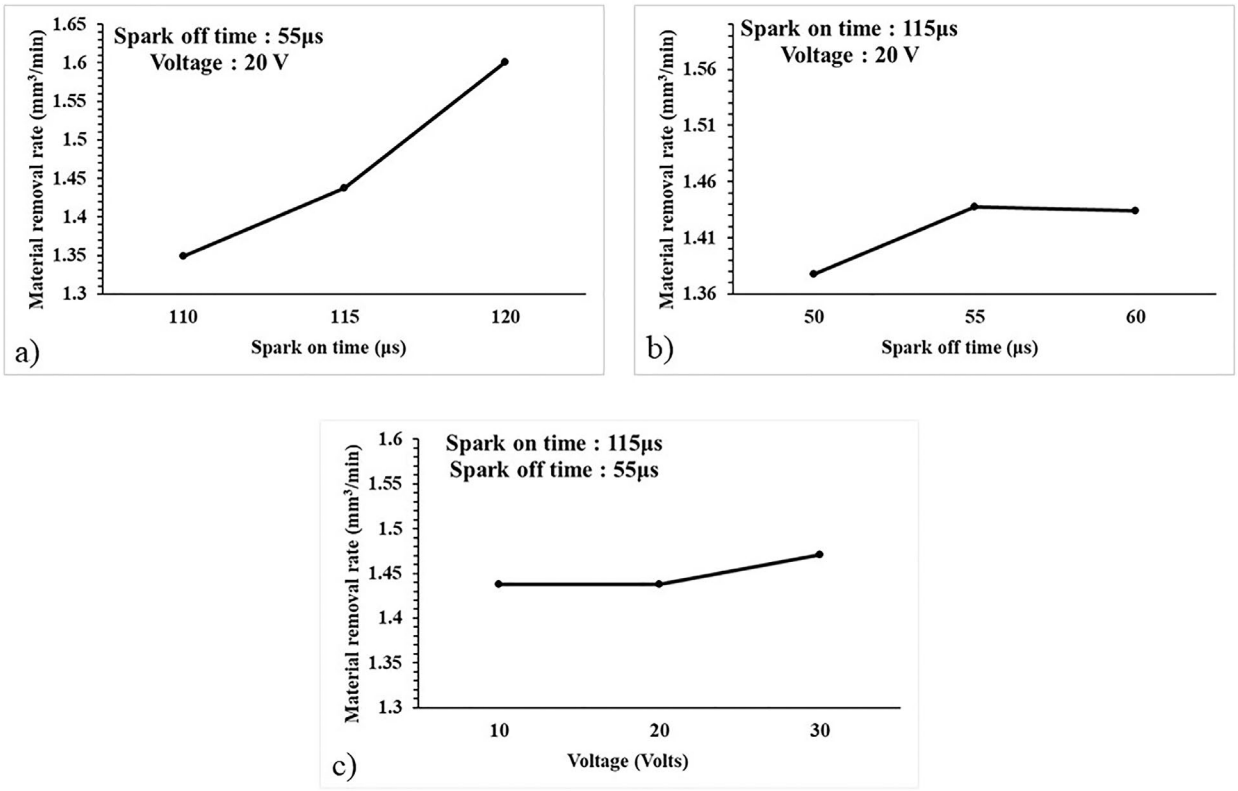

Fig. 4. Graphical plots of surface roughness when varied (a) S_{ON} time (b) S_{OFF} time and (c) voltage

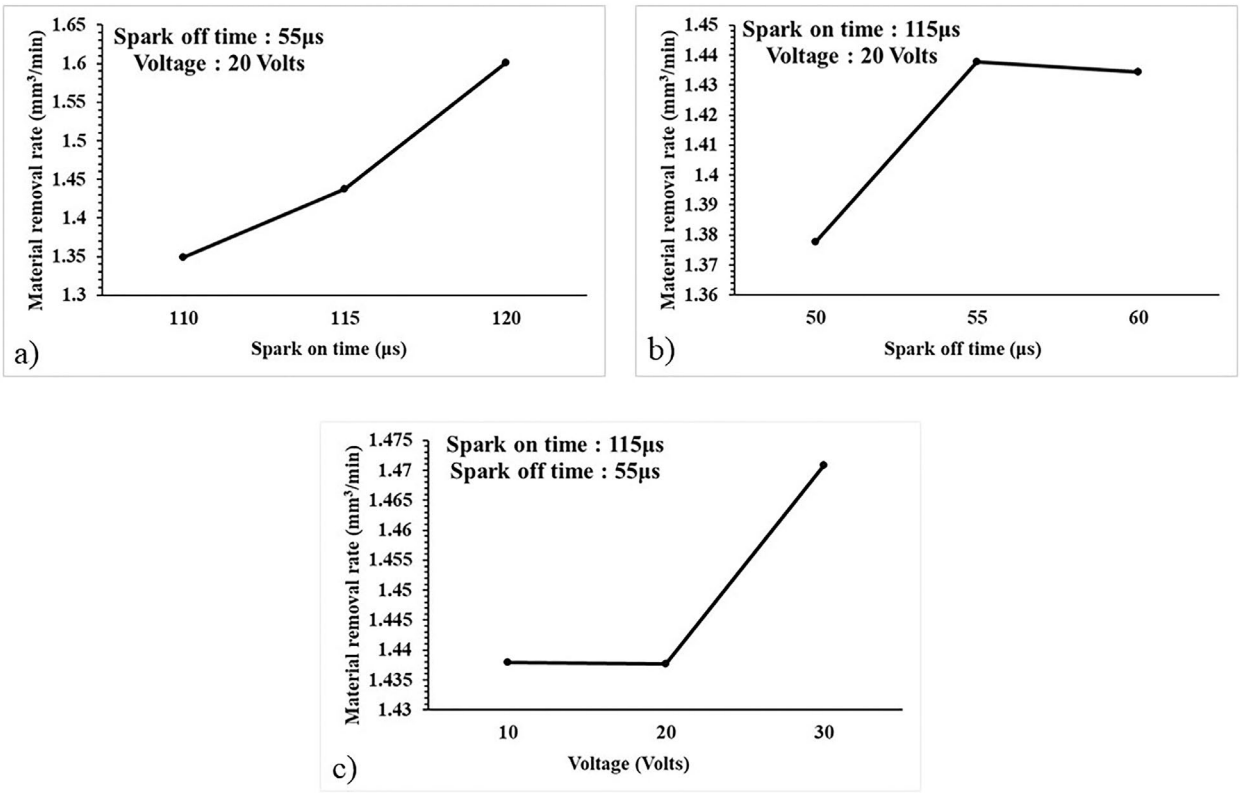

Fig. 5. Graphical plots of Material Removal Rate (MRR) when varied (a) S_{ON} time (b) S_{OFF} time and (c) voltage

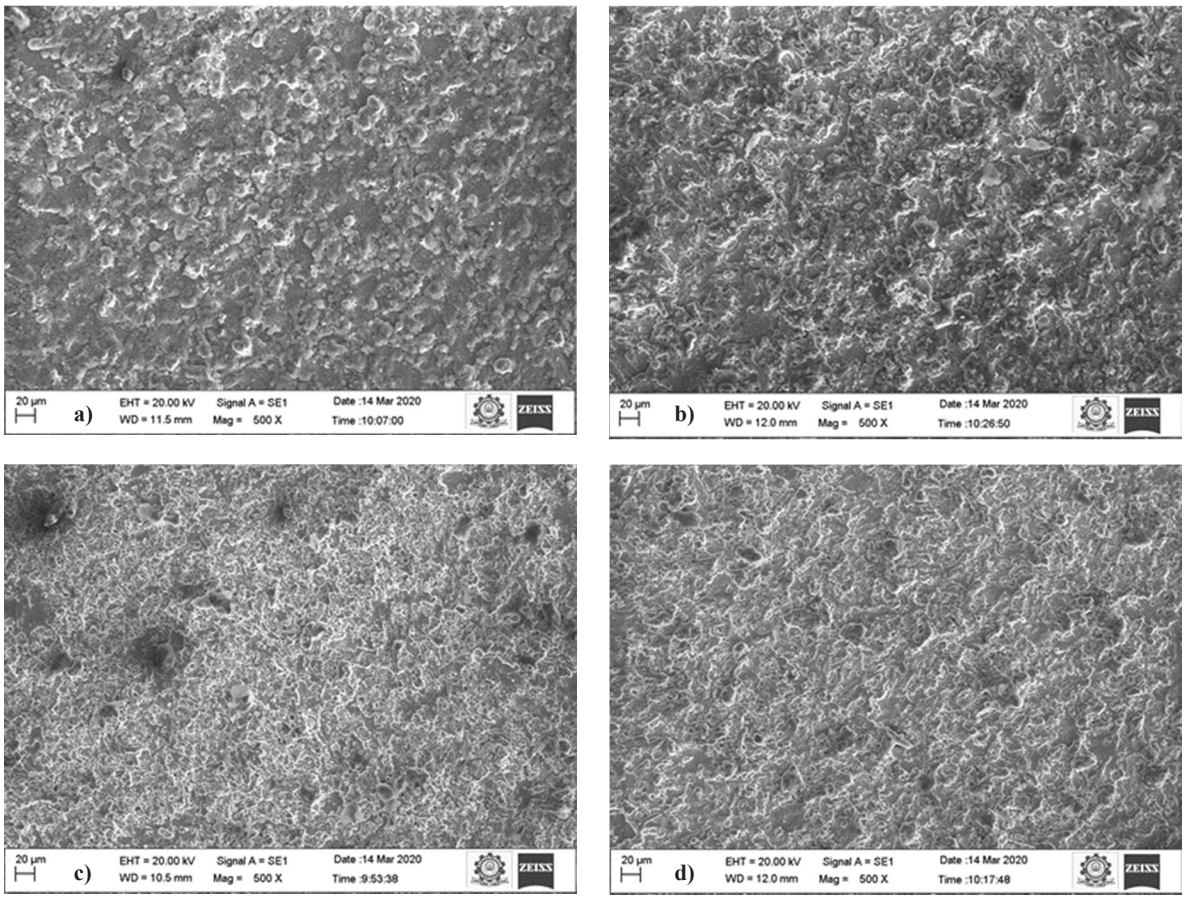

Fig. 6. SEM images of the machined surface for different combinations of machined conditions: (a) S_{ON} = 110 µs, S_{OFF} = 50 µs, and voltage = 30 V (b) S_{ON} = 120 µs, S_{OFF} = 60 µs, and voltage = 10 V (c) S_{ON} = 110 µs, S_{OFF} = 50 µs, and voltage = 10 V, and (d) S_{ON} = 120 µs, S_{OFF} = 55 µs, and voltage = 30 V

white cast layer [6] on the machined surface was clearly visible. Fig. 6(a) and Fig. 6(b) display the SEM images of the surface with minimum and maximum SR values respectively. The surface irregularity of the machined surface could be due to the deposition of the molten metal during the machining process. At a machining condition of S_{ON} = 120 µs, S_{OFF} = 60 µs, and voltage = 10 V, the spark lasted for the maximum period enabling the deep erosion but the lower intensity of the spark resulted in less vaporization of the Ni-Ti alloy. During the spark OFF time, the partially vaporized metal solidified and deposited over the surface resulting in the maximum irregularity. On the other hand, at a machining condition of S_{ON} = 110 µs, S_{OFF} = 50 µs, and voltage = 30 V, the surface irregularity was minimum and this could be due to a combination of shorter spark ON and OFF times and higher spark intensity.

Similarly, Figs 6(c) and 6(d) represents the SEM images of the machined surface when the MRR values were minimum and maximum respectively. The combination of machining parameters with S_{ON} = 120µs, S_{OFF} = 55µs, and voltage = 30 V (Fig. 6(d)) provided longer spark ON time and high spark intensity caused higher melting and vaporization of the material. This condition also symbolized the formation of larger intensity of white cast layer resulted from the faster material removal. For the same reason, the surface profile did not show much irregularity.

While machining, the electro spark induced at minimum pulse on has high intensity to fuse and vaporize the material. Due to the increase in pulse time, the intensity of the spark was prolonged leading to diffusion of the workpiece material and increased MRR was found. It was inclined towards the current density, which was generated due to the discharge current [8,9]. However, for maximum pulse on time, the material behavior varied and it started to conduct the energy between the electrode and work. The presence of carbon (alloying element) in the SMA alloy facilitated the material to have high electrical conductivity. Specifically, for prolonged electro spark the presence of carbon in the SMA intended to conduct the amount of energy used. During machining the high conductivity of the material leads to transform energy (electrical conductivity) between the electrode (copper material) and the SMA work material [29,30]. It also inhibited the production of electro spark and the intensity of the spark turned weak and form inefficient process. During electro spark production, the electrode or the tool used becomes vulnerable with respect the machining conditions.

Furthermore, the surface characterization revealed the formation of globules, microcrack, craters, and micro voids on the recast layer due to the thermal stress developed during the machining of Ni-Ti alloy. The thermal conductivity of the Ni-Ti alloy was less and the workpiece got heated during the spark ON time and suddenly got cooled during the spark OFF time under the di-electric medium might be the reason for the generating the thermal stress. The SEM micrographs in Fig. 7, illustrates the

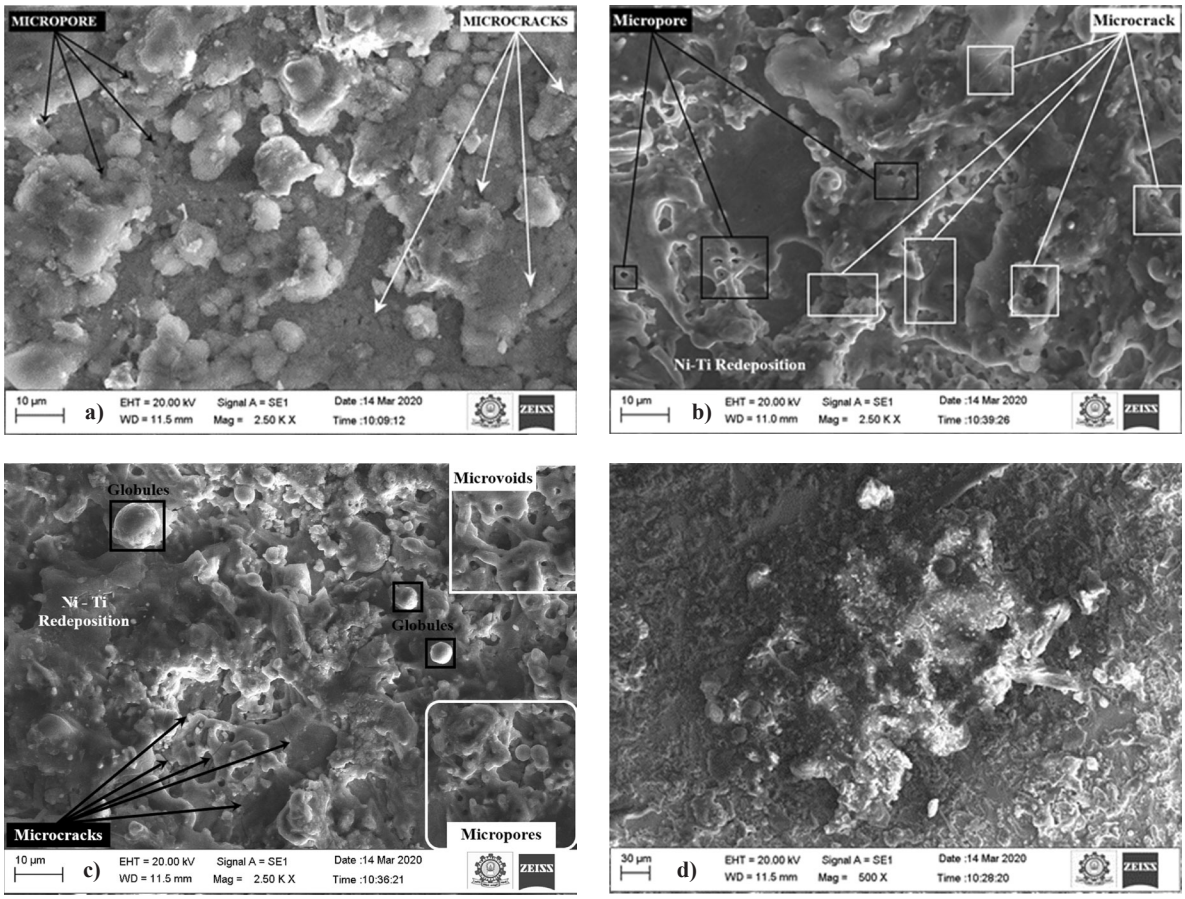

Fig. 7. Surface topography for different machining conditions revealing (a) micro pores and cracks at S_{ON} 110 µs and voltage 30 V (b) micro pores and cracks at S_{ON} 115 µs and Volt 30v (c) micro pores and cracks at S_{ON} 120 µs and voltage 30 V (d) cluster of debris at S_{ON} 120 µs and voltage 30 V

surface topology of the machined component for the machining conditions for different S_{ON} times: 110 µs, 115 µs, and 120 µs. For S_{ON} time 110 µs, the micro voids and cracks were present over the recast layer. The pores/voids were visible on the surface but their concentrations were lower and the debris globules attached over the surface might initiate the crack. However, the bond between the recast compound and surface was weak and hence the crack would not be able to penetrate the substrate. The voids and cracks were highlighted in the SEM images.

Fig. 7(b) clearly demonstrated evidences of the micropores and microcracks on the surface and this could be due to higher spark energy. The thermal energy generated by the spark melted the metal surface and created craters over the surface. The temperature on the surface was elevated during spark ON and at the same time the flushing suddenly cooled the surface. Owing to the low heat-conducting capacity of the Ni-Ti alloy, this caused an uneven distribution of temperature, which generated the thermal stresses on the surface and recasts layer leading to an initiation of the cracks. The voids and cracks formed during the machining under the condition S_{ON} time 120 µs is presented in Fig. 7(c). As the S_{ON} time increased, the micro crack appeared over the surface was concentrated compared to the other S_{ON} times. The surface defect at the higher machining condition S_{ON} time (120 µs) and voltage (30 V), the thermal energy was high enough to melt and vaporize the material and cluster of debris attached to the surface as seen in Fig. 7(d). Similar research on machining nickel titanium alloy revealed with a voids and pores due to the influence of spark intensity [31]. In addition, the machining time (pulse duration and wire feed) has also influenced the surface quality of the machining process.

The Energy Dispersive Spectroscopy (EDS) result revealed that the presence of the elements Nickel, Titanium, Oxygen, Carbon, Copper, Zinc and some traces of other elements. The elemental weight percentages from the EDS for both S_{ON} time 110 µs and 120 µs is presented in Fig. 8(a) and Fig. 8(b) respectively. The higher weight percentages of Nickel and Titanium for both S_{ON} times (i.e., 110 µs and 120 µs) reflected the fact that these elements were the major constituents of the workpiece material. The presence of oxygen on the surface of machined samples for both S_{ON} times could be due to the result of oxidation taking place during the machining process. The weight percentage of the Oxygen was comparatively high for the lower S_{ON} time (i.e., 110 µs) and vice versa. This clearly presented that more oxides formed for the lower S_{ON} time (i.e., 110 µs). The presence of Cu and Zn resulted due to the deposition of the tool material during the machining process. In both cases considerably small amount of Cu and Zn deposited over the surface favoured the theory that very small amount of tool materials during the spark present in the plasma got diffused on the surface.

The presence of the carbon could due to the heating of material by means of spark during the machining. As the spark melts the material, the same thermal energy overheated the di-electric medium resulting in the formation of carbon on the surface of the material. The experimental results favoured the theory as the percentage of C was less for the low S_{ON} time compared to the high S_{ON} time. This might be due to the fact that at higher S_{ON}

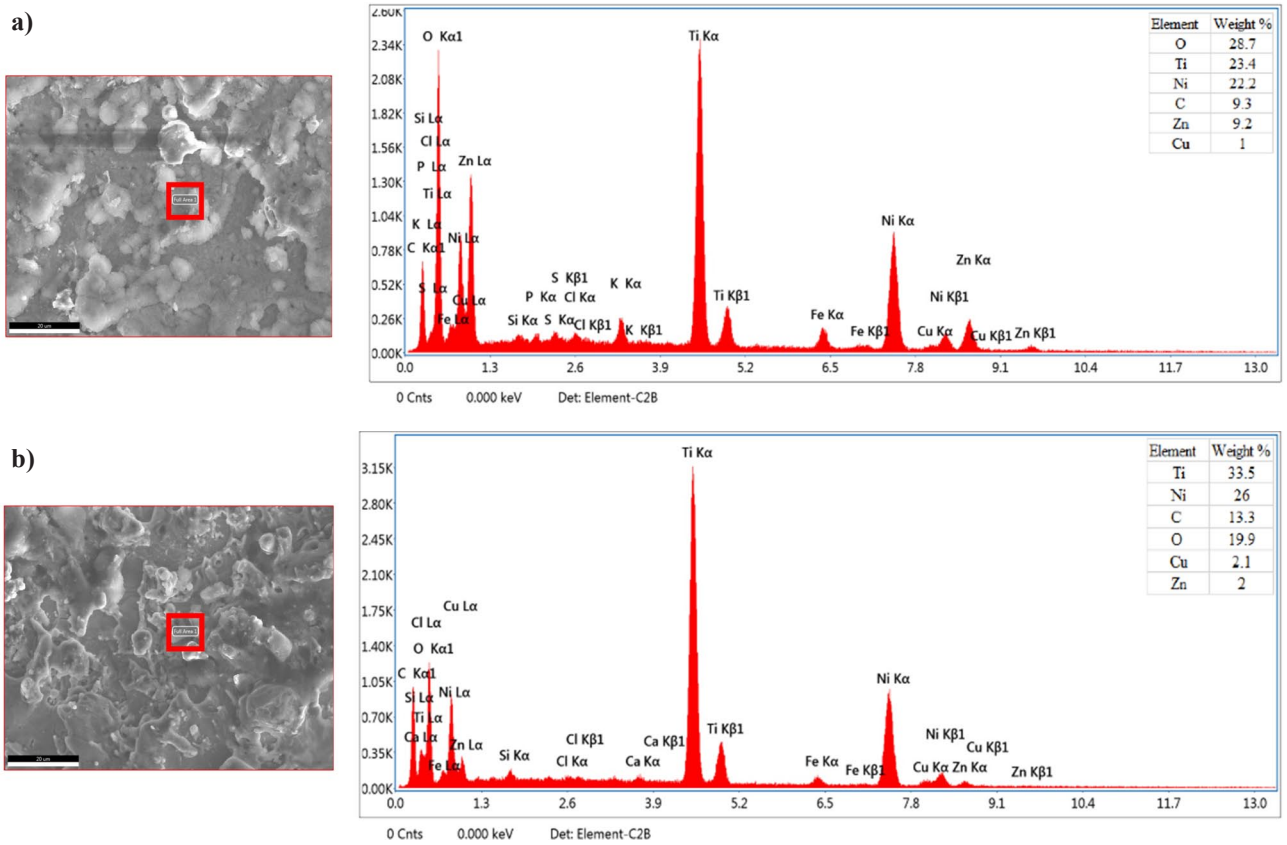

Fig. 8. EDS for (a) S_{ON} time of 110 µs and (b) S_{ON} time of 120 µs with a voltage of V and S_{OFF} time of µs

time the spark energy lasted for maximum time and heated the di-electric medium more than hat at low S_{ON} time. The traces of the other elements could come from the di-electric medium. The image mappings of the major constituents in the machined surface for S_{ON} time 110 µs and 120 µs are presented in Figs 9(a) and 9(b) respectively. The mappings revealed that the surface of the S_{ON} time 110 µs was rich in oxygen compared to the S_{ON} time of 120 µs and this supported the quantitative values obtained from EDS. It was clear to infer that the presence of Ti element was uniformly distributed over the machined surface along with oxygen element. It was also noted that the presence of nickel element was dominated but less than the titanium over the machined surface. The aforesaid information was highly supporting the theory of forming titanium oxide. The presence of titanium – oxygen in the bio environment (body fluid) has high resistance towards corrosion and material degradation for biomedical application [29,30].

3.4. General discussions

In summary, both SR and MRR increased with the increase in S_{ON} time. The presence of the micro voids, micro cracks and globules in the white cast layer on the machined

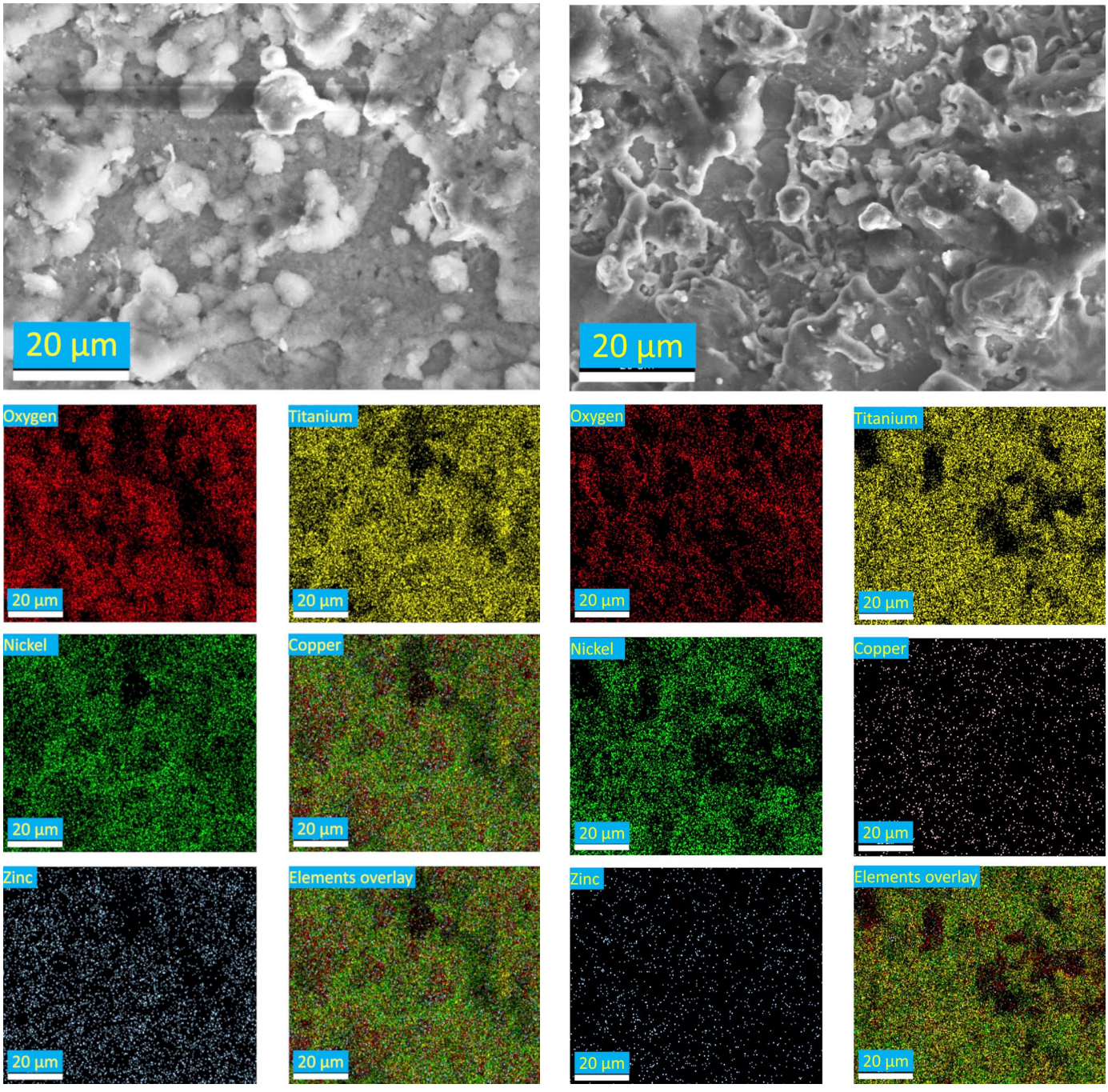

a) b)

Fig. 9. EDS spectrum and image mapping with S_{ON} times of (a) 110 µs and (b) 120 µs

surface was clearly visible in the SEM images. The concentration of the micro cracks and voids increased with the increase in the impact of thermal energy (i.e., S_{ON} time). The elements present (i.e., O, Cu and C) in the machined surface other than the elements of the parent alloy could be due to the machining process. The presence of oxygen favoured the theory of formation of oxides over the surface and carbon due to the heating of specimen surface and reaction of di-electric with the molten material during flushing. The optimum parametric setting for the minimum SR was 110 µs Spark ON time, 55 µs Spark OFF time and 30 V. Similarly, the optimum parametric setting for the maximum MRR was 120 µs Spark ON time, 55µs Spark OFF time and 30 V of voltage. It was understood that the machining of low carbon NiTi alloy was recommended to process at 110 µs – 55 µs – 30 V (S_{ON} – S_{OFF} – V), to achieve better surface roughness with minimal surface damage. Furthermore, for the same machining condition, the maximum surface oxide formation on the low carbon NiTi alloy was achieved for biomedical applications. Kumar et al [21] reported that while machining the implant material (titanium alloy) with the presence of titanium oxide over the machined surface demonstrated high corrosion resistance and surface protection simulated under bio fluids.

4. Conclusions

This work comprehensively studied the effects of process parameters such as Spark ON time (S_{ON}), Spark OFF time (S_{OFF}), and voltage (V) on the response, surface properties and productivity while machining low carbon NiTi alloy using Wire Electro Spark Erosion (WESE) process. Based on the results, it was concluded that S_{ON} time increased both the surface roughness (SR) and material removal rate (MRR). However, an increase in voltage reduced surface roughness but increased MRR. The minimum SR (2.168 µm) found at a machining condition of S_{ON} = 110 µs, S_{OFF} = 50 µs, and voltage = 30 V. The maximum MRR (1.616 mm^3/min) found at a machining condition of S_{ON} = 120 µs, S_{OFF} = 55 µs, and voltage = 30 V. The presence oxygen over the machined surface indicated the formation of surface oxides caused by the input thermal energy during the machining process. The weight percentage of the C increased with the S_{ON} time due to the combined effect of heating the Ni-Ti surface and the Dielectric medium. Based on the results obtained, WESE could be suitable process for machining low carbon NiTi alloy with good surface finish and higher productivity.

REFERENCE

[1] R. Chaudhari, J.J. Vora, V. Patel, L.N.L. de Lacalle, D.M. Mater. (Basel) **13**, 1-13 (2020). DOI: https://doi.org/10.3390/ma13030530

[2] C. Velmurugan, V. Senthilkumar, S. Dinesh, D. Arulkirubakaran, Mach Sci Technol **22**, 355-401 (2018). DOI: https://doi.org/10.1080/10910344.2017.1365894

[3] M. Manjaiah, S. Narendranath, S. Basavarajappa, Trans. Nonferrous. Met. Soc. China **24**, 12-21 (2014). DOI: https://doi.org/10.1016/S1003-6326(14)63022-3

[4] A.M. Takale, N.K. Chougule, Mater. Sci. Eng. C **97**, 264-274 (2019). DOI: https://doi.org/10.1016/j.msec.2018.12.029

[5] Shih-Fu Ou, Bou-Yue Peng, Yi-Cheng Chen, Meng-Hsiu Tsai, Met. **8**, 342-354 (2018). DOI: https://doi.org/10.3390/met8050342

[6] J.F. Liu, Y.B. Guo, T.M. Butler, M.L. Mater. Des. **109**, 1-9 (2016). DOI: https://doi.org/10.1016/j.matdes.2016.07.063

[7] S.A. Sonawane, M.L. Kulkarni, J. King. Saud. Univ. Eng. Sci. **30**, 250-258 (2018). DOI: https://doi.org/10.1016/j.jksues.2018.04.001

[8] S. Kumar, A. Batish, R. Singh, A, Wear **386-387**, 223-229 (2017). DOI: https://doi.org/10.1016/j.wear.2017.01.067

[9] H. Soni, S. Narendranath, M.R. Ramesh, Silicon **10**, 2483-2490 (2018). DOI: https://doi.org/10.1007/s12633-018-9780-9

[10] H. Soni, N. Sannayellappa M.R. Ramesh, J. Mater. Res. **32**, 1-9 (2017). DOI: https://doi.org/10.1557/jmr.2017.137

[11] M.H. Elahinia, M. Hashemi, M. Tabesh, S.B. Bhaduri, Prog. Mater. Sci. **57**, 911-946 (2012). DOI: https://doi.org/10.1016/j.pmatsci.2011.11.001

[12] K. Mouralova, L. Benes, J. Bednar, R. Zahradnicek, T. Prokes, Z. Fiala, Coat **10**, 590-610 (2020). DOI: https://doi.org/10.3390/coatings10060590

[13] S.S. Nain, D. Garg, S. Kumar, Eng. Sci. Technol. Int. J. **20**, 247-264 (2017). https://doi.org/10.1016/j.jestch.2016.09.023

[14] S. Nemat-Nasser, J.Y. Choi, W.G. Guo, J.B. Isaacs, Mech. Mater. **37**, 287-298 (2005). DOI: https://doi.org/10.1016/j.mechmat.2004.03.007

[15] T.R Newton, S.N. Melkote, T.R. Watkins, R.M. Trejo, L. Reister, Mater. Sci. Eng. A **513**, 208-215 (2009). DOI: https://doi.org/10.1016/j.msea.2009.01.061

[16] S.L. Chen, S.F. Hsieh, H.C. Lin, M.H. Lin, J.S. Huang, Mater. Sci. Eng. A **445**, 486-492 (2007). DOI: https://doi.org/10.1016/j.msea.2006.09.109

[17] M. Manjaiah, S. Narendranath, S. Basavarajappa, V.N. Gaitonde, Precis. Eng. **41**, 68-77 (2015). DOI: https://doi.org/10.1016/j.precisioneng.2015.01.008

[18] Y. Sun, Y. Gong, Y. Liu, Q. Li, Y. Zhou, Arch. Civ. Mech. Eng. **17**, 964-977 (2017). DOI: https://doi.org/10.1016/j.acme.2017.02.004

[19] R. Chalisgaonkar, J.J. Kumar, Brazilian Soc. Mech. Sci. Eng. **38**, 883-911 (2016). DOI: https://doi.org/10.1007/s40430-015-0335-3

[20] A.M.A. Al-Ahmari, M.S. Rasheed, M.K. Mohammed, T. Saleh, Mater. Manuf. Process **31**, 447-455 (2016). DOI: https://doi.org/10.1080/10426914.2015.1019102

[21] S. Kumar, M.A. Khan, B. Muralidharan, Mater. Manuf. Process **34**, 695-700 (2019). DOI: https://doi.org/10.1080/10426914.2019.1566609

[22] H. Bisaria, P. Shandilya, Mater. Manuf. Process **33**, 977-985 (2018). DOI: https://doi.org/10.1080/10426914.2017.1388518

[23] A. Roy, S. Narendranath, Mater. Res. Exp. **5**, 125701-125715 (2018). DOI: https://doi.org/10.1088/2053-1591/aaddee.

[24] K. Mouralova, J. Kovar, L. Klakurkova, T. Prokes, H. Horynova, Measurement **104**, 12-20 (2017).
DOI: https://doi.org/10.1016/j.measurement.2017.03.009

[25] N.K. Gupta, N. Somani, C. Prakash, R. Singh, A.S. Walia, S. Singh, C.I Pruncu, Mater. **14**, 2292 (2021).
DOI: https://doi.org/10.3390/ma14092292

[26] Y.S Liao, J.T Huang, Y.H Chen, J. Mater. Process. Technol. **149**, 165-171 (2004).
DOI: https://doi.org/10.1016/j.jmatprotec.2003.10.034

[27] R. Chaudhari, J.J. Vora, S.S.M. Prabu, I.A. Mani, V.K. Patel, D.M. Parikh, Adv. Manuf. **9**, 64-80 (2021).
DOI: https://doi.org/10.1007/s40436-019-00267-0

[28] V.N. Kulkarni, V.N. Gaitonde, S.R. Karnik, M. Manjaiah, J.P. Davim, Mater. **13**, 2184 (2020).
DOI: https://doi.org/10.3390/ma13092184

[29] S. Sivakumar, M. Adam Khan, B. Muralidharan, L. Muthulakshmi, Mater. Today Proc. **22**, 3226-3231 (2020).
DOI: https://doi.org/10.1016/j.matpr.2020.03.461

[30] S. Sivakumar, M. Adam Khan, Giftson J. Senapathy, J. Bio. Tribo. Corr. **6**, 1-11 (2020).
DOI: https://doi.org/10.1007/s40735-020-0326-5

[31] H Bisari, P Shandilya, J. Mat. Res. **35**, 537-558 (2020).
DOI: https://doi.org/10.1557/jmr.2020.32